Thesis for the degree of Licentiate of Technology, Sundsvall 2009

Nanoscaled Structures in Ruthenium Dioxide Coatings

Christine Malmgren

Supervisors:
Prof. Håkan Olin
Associate Prof. Joakim Bäckström

Department of Natural Sciences, Engineering and Mathematics
Mid Sweden University, SE-851 70 Sundsvall, Sweden

ISSN 1652-8948
Mid Sweden University Licentiate Thesis 36
ISBN 978-91-86073-33-6

Akademisk avhandling som med tillstånd av Mittuniversitetet i Sundsvall framläggs till offentlig granskning för avläggande av teknologie licentiatexamen fredagen den 27 mars, 2009, klockan 13:15 i sal O102, Mittuniversitetet Sundsvall. Seminariet kommer att hållas på svenska.

Nanoscaled Structures in Ruthenium Dioxide Coatings
Christine Malmgren

Department of Natural Sciences, Engineering and Mathematics
Mid Sweden University, SE-851 70 Sundsvall
Sweden

Telephone: +46(0)771-975 000

Typeset by the author using LaTeX 2_ε.
Printed by Kopieringen Mid Sweden University, Sundsvall, Sweden, 2009

Nanoscaled Structures in Ruthenium Dioxide Coatings

Christine Malmgren

Department of Natural Sciences, Engineering and Mathematics
Mid Sweden University, SE-851 70 Sundsvall, Sweden
ISSN 1652-8948, Mid Sweden University Licentiate Thesis 36;
ISBN 978-91-86073-33-6

Abstract

An essential ingredient in the generation of environmentally compatible pulp bleaching chemicals is sodium chlorate. Chlorate is produced in electrochemical cells, where the electrodes are the key components. In Sweden the so-called DSA ® electrodes with catalytic coatings have been produced for more than 35 years. The production of chlorate uses a large amount of electric energy, and a decrease of just five percent of this consumption would, globally, decrease the consumption of electrical energy corresponding to half a nuclear power reactor. The aim of this project is to improve the electrode design on the nanoscale to decrease the energy consumption.

The success of the DSA® depends on the large catalytic area of the coating, however, little is known about the actual structure at the nanometer level.

To increase the understanding of the nanostructure of these coatings, we used a number of methods, including atomic force microscopy, transmission electron microscopy, X-ray diffraction, porosimetry, and voltammetric charge. We found that the entire coating is built up of loosely packed rutile mono-crystalline $20 - 30$ nm sized grains. The small grain sizes give a the large area, and consequently, lower cell-voltage and reduced energy consumption. A method to control the grain size would thus be a way to control the electrode efficiency.

To alter the catalytically active area, we made changes in the coating process parameters. We found a dependency of the crystal-grain sizes on the choice of ruthenium precursor and processing temperature. The use of ruthenium nitrosyl nitrate resulted in smaller grains than ruthenium chloride and lowering the temperature tended to favour smaller grains.

A more radical way would be to create a totally different type of electrode, manufactured in another way than using the 1965 DSA ® recipe. Such new types of electrodes based on, for example, nanowires or nanoimprint lithography, are discussed as future directions.

Keywords: Bleaching chemicals, sodium chlorate, ruthenium dioxide, electrodes, crystallites, nanowires, microscopy, diffraction, electrocatalytic area, reduced energy consumption

Sammanfattning

Natriumklorat är en av huvudingredienserna för att bleka pappersmassa på ett miljövänligt sätt. Klorat tillverkas genom elektrolys i stora elektrokemiska celler, där en nyckelkomponent är elektroderna. Dessa så kallade dimensionsstabila anoder med katalytisk beläggning har tillverkats i Sverige i över 35 år. Kloratproduktionen kräver stora mängder elektrisk energi, och en minskning med så lite som fem procent skulle, globalt sett, minska energiförbrukningen motsvarande en halv kärnreaktor. Målet med det här projektet är att förbättra elektroddesignen på nanonivå för att minska energiförbrukningen.

Framgången med DSA® beror på den stora katalytiska ytan i beläggningen, dock vet man inte så mycket om den faktiska strukturen på nanometernivå.

För att öka förståelsen för nanostrukturen av de här beläggningarna har vi använt ett flertal metoder; bland annat atomkraftmikroskopi, transmissionselektronmikroskopi, röntgendiffraktion, porosimetri och cyklisk voltammetri. Vi kom fram till att hela beläggningen består av löst packade en-kristallina korn med rutilstruktur, med en diameter på $20 - 30$ nm. Mindre korn ger en större yta och följdaktligen lägre cellspänning och lägre energiförbrukning. Om man kan styra kornstorleken skulle man alltså kunna styra elektrodens effektivitet.

För att ändra den katalytiskt aktiva ytan gjorde vi förändringar av parametrarna i beläggningsprocessen. Vi kom fram till att kornstorleken beror av ursprungskemikalien och oxideringstemperaturen. Om man använder rutenium-nitrosylnitrat kan man åstadkomma mindre korn än om man använder rutenium-klorid, förutsatt att man har en låg temperatur i ugnen.

Ett mer radikalt sätt vore att tillverka en helt annan typ av elektrod än den man får via receptet från 1965. Exempel på en sådan elektrod är något som bygger på nanotrådar eller nanoimprintlitografi, vilket vi diskuterar som möjliga framtida inriktningar.

Acknowledgement

FIRST OF ALL I would like to thank my supervisors Håkan Olin and Joakim Bäckström, for interesting discussions and encouragement. I would also place a thank to Permascand AB for supplying me with electrode material and letting me use their lab, all helpful employees always making me feel welcome, and especially to Susanne Holmin, Fredrik Herlitz and Lars-Åke Näslund for valuable discussions. And thanks also to Babak Heidari and Marc Beck at Obducat AB for theoretical and experimental guidance regarding imprint. The KK-foundation is acknowledged for financial support.

I am grateful for all assistance with experiments and interpretation of the results I have got from a number of people, including my article co-writers. I would also like to thank my co-workers, family and friends for believing in me, and finally
Magnus, thank you for being in my life.

List of Figures

1.1 Photo of anode-package 2
1.2 Schematic picture of chlorate-cell 5

2.1 Electron interaction with specimen 8
2.2 Scanning electron microscope setup 9
2.3 Transmission electron microscope setup 11
2.4 Beam path in TEM 12
2.5 Atomic force microscope setup 14

4.1 SEM image of ”cracked-mud” structure 24
4.2 SEM and TEM images of coating in cross section 24
4.3 AFM and TEM images of grains 26
4.4 X-ray diffraction pattern and measurements of crystallite sizes . 27
4.5 AFM images of thin film electrode 30
4.6 SEM cross section image of thin film electrode 30
4.7 Ellipsometric result 31

5.1 Different stages of nanowires 35
5.2 Principle of nanoimprint lithography 36
5.3 Micrograph of sol-gel coating 36

List of papers

1. Nanoscale characterization of crystallinity in DSA® coating
   C. Malmgren, M. Hummelgård, J. Bäckström, A. Cornell and H. Olin
   J. Phys.: Conf. Ser. 100 (2008) 052026.

2. Nanocrystallinity in RuO_2 coatings – influence of precursor and preparation temperature
   C. Malmgren, A. K. Eriksson, A. Cornell, J. Bäckström, S. Eriksson and H. Olin
   Submitted manuscript

Contents

Abstract i

Sammanfattning iii

Acknowledgement v

List of figures vii

List of papers ix

1 Introduction 1
- 1.1 Background . . . 2
- 1.2 The history and development of the DSA® . . . 3
- 1.3 Sodium chlorate - production and use . . . 4
- 1.4 Materials used in the electrochemical system . . . 5

2 Microscopy 7
- 2.1 Electron interaction with specimen . . . 7
- 2.2 Scanning electron microscopy . . . 8
- 2.3 Transmission electron microscopy . . . 10
  - 2.3.1 Electron diffraction . . . 12
- 2.4 Atomic force microscopy . . . 13

3 Other characterisation methods 17
- 3.1 Porosimetry . . . 17
- 3.2 X-ray diffraction . . . 18
- 3.3 Cyclic voltammetry . . . 19
- 3.4 Spin-coating . . . 19
- 3.5 Ellipsometry . . . 20

4 Summary of papers 23

4.1 Cracked mud structure 23
4.2 Nanoscaled characterisation of DSA® – Paper I 25
4.3 Dependency on process parameters – Paper II 26
4.4 Thin films – toward nanopatterned electrodes 29

5 Future work **33**
5.1 Nanowire growth 33
5.2 Nanoimprint lithography 34
5.3 Sol-gel based coating solution 37
5.4 Discussion 37

6 Conclusion **39**

Bibliography **41**

Bumblebees can't fly
they just don't know it

Chapter 1

Introduction

AN ESSENTIAL INGREDIENT in the generation of environmentally compatible pulp bleaching chemicals is sodium chlorate. The chlorate is produced in electrochemical cells, where the electrodes are key components. The anodes, called Dimensionally Stable Anodes (DSA®), consist of titanium substrates coated with a mix of titanium- and ruthenium dioxide (typically $Ti_{0.7}Ru_{0.3}O_2$). The cathodes are made of steel. The production of chlorate uses large amounts of electric energy, and a decrease of just five percent of this consumption would, globally, decrease the electrical energy consumption corresponding to half a nuclear power reactor.

The aim of this project is to improve the electrode design in order to decrease the energy consumption. The goals are to gain knowledge about the feasibility of a new generation of electrodes. The project involves the electrode manufacturing company Permascand and the nanoimprint company Obducat.

In this project the existing anode coating, produced today, has been studied down to the nanoscale. Ruthenium dioxide prepared in laboratory with variations of the preparation conditions have been studied as a model system, and attempts to physically increase the anode surface area have been performed.

Figure 1.1: Photo of anode package for chlorate production. The electrodes are usually assembled in electrode packages with anodes on one side and cathodes on the other side, or just the anodes in the package using the cell-box as cathode. The latter is the case in this photo. Photo reproduced with permission from Permascand.

1.1 Background

The Dimensionally Stable Anode (DSA®) was developed in the mid 1960's. The invention provided lower cell-voltage, longer electrode lifetime, better product quality and mostly, more stable production conditions, for the chlor-alkali and chlorate industry. The principle is a titanium plate coated with a catalytic precious metal oxide. Figure 1.1 shows a photo of an anode package. The success of the DSA® technique is said to depend on the large catalytic area of the anode coating together with metallic conductivity of the precious metal oxide. The two most frequently used oxides for the coating, ruthenium dioxide and iridium dioxide, are known to be metallic conductors over the whole accessible range of temperature [1]. The coating has an effective surface areas that are $10 - 1000$ times larger than the apparent surface, resulting in superior electrocatalytical properties [2].

In Sweden DSA® electrodes have been produced for more than 35 years and hence helped saving energy corresponding to the yearly production of one nuclear power station [3].

1.2 The history and development of the DSA®

The DSA® as known today was patented by Beer [4] in 1965. Typically an anode consists of a titanium plate, some millimetres thick, coated on both sides with about 10 micrometers of a mixed oxide of ruthenium and titanium ($Ru_{0.3}Ti_{0.7}O_2$). The name "dimensionally stable" comes from the electrodes used in chlorate production prior to the invention of the DSA®; graphite blocks. In use, the graphite block is slowly consumed to form CO_2 and therefore the electrode gap (between anode and cathode) is not constant, but has to be adjusted many times. The invention of the DSA® gave the advantage of an electrode that is not consumed during the process so that the electrode gap does not need to be adjusted. The coating of the DSA® eventually stops working (a typical lifetime is about ten years) and has to be replaced, but the dimensions of the anode are constant. The anodes are therefore called dimensionally stable anodes.

By the mid 1950s high quality titanium started to be produced, it was noticed to have good electrochemical properties and good corrosion resistance. However, in some aqueous halide solutions titanium shows a tendency to corrode. J.B. Cotton (head of research and development at a British company called ICI) experimented with attaching other metals to the titanium in order to minimize that risk and in 1958 he found that when spot welding a small piece of platinum wire to the titanium, current passed through the platinum. The concept of the platinum coated titanium bielectrode had thus been recognized. Totally independent of the ICI work, an employee of Magneto Chemie in The Netherlands, H.B. Beer, had taken out a patent on rhodium-plated titanium. Its priority was just a few weeks before that of the ICI patent. Two years later Angell (ICI) proposed an alternative to electrodepositing of coatings. His method was to take a solution containing a soluble noble metal salt, apply it as paint to the titanium surface and then heat it in air to decompose the salt to the metallic state. The consequence of the two 1958 patents was an agreement between Magneto Chemie and ICI, under which the development of titanium-based electrodes to replace graphite electrodes in chlorine cells was to be shared. Beer was to work on coating formulations, while others were to concentrate upon assessing the commercial viability of the coatings on titanium electrodes. The agreement stayed in force for several years, not being terminated until 1965, when Beer filed the patent of ruthenium oxide coating. [5] - [7]

1.3 Sodium chlorate - production and use

The largest market for DSA® electrodes is in the chlor-alkali industry, electrolysis of NaCl to gaseous chlorine with simultaneous production of NaOH and hydrogen. However, the anodes are also used in chlorate mills to produce sodium chlorate ($NaClO_3$). Most of the sodium chlorate produced today (up to 95 %) is used for producing chlorine dioxide (ClO_2) that is used for bleaching of pulp and paper. Sodium chlorate is also used in chemical oxygen generators in for example commercial aircrafts to provide emergency oxygen to passengers in case of drops in cabin pressure.

Industrially, sodium chlorate is synthesised from the electrolysis of sodium chloride solution: sodium chloride is oxidized to sodium chlorate and water is reduced to hydrogen gas (figure 1.2). The electrolyte contains, beside brine ($NaCl(aq)$), also some hydrochloric acid (HCl) to give a proper pH and sodium dichromate ($NaCr_2O_7$) which forms a protective film on the cathode. [8, 9]

$$NaCl + 3H_2O \rightarrow NaClO_3 + 3H_2 \tag{1.1}$$

More specific on the anode; chlorine is formed as in reaction 1.2. The chlorine is then dissolved to hypo-chlorous acid in the electrolyte (reaction 1.3) which is then transformed to chlorate, according to reactions 1.4 and 1.5.

$$2Cl^- \rightarrow Cl_2 + 2e^- \tag{1.2}$$

$$Cl_2 + H_2O \rightarrow ClOH + Cl^- + H^+ \tag{1.3}$$

$$ClOH \leftrightarrow ClO^- + H^+ \tag{1.4}$$

$$2ClOH + Cl^- \rightarrow ClO_3^- + 2H^+ + 2Cl^- \tag{1.5}$$

Chlorate was produced by electrosynthesis for the first time by Wilhelm von Hisinger and Jöns Jakob Berzelius [10] in 1802 . They were performing ”experiments relating to the effect of the electrical pile on salts and their bases”. In one of the series, sodium chloride solution was electrolysed between silver wires. In the remaining clear solution they found sodium chloride, silver chloride and ”perhaps, hyperoxygenized muriatic sodium and a formerly unknown silver salt”. In fact, the salts were sodium chlorate and silver chlorate.

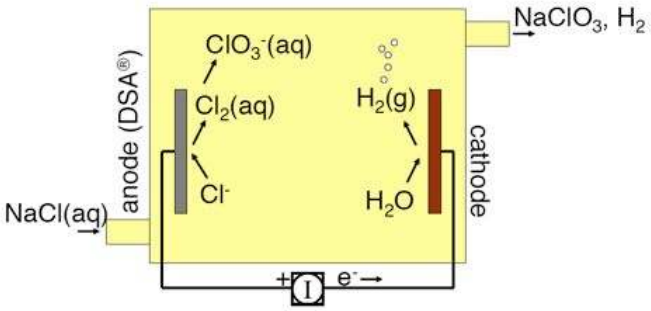

Figure 1.2: Schematic picture of chlorate-cell. Sodium chloride and water is pumped in on the anode side, while the sodium chlorate (in water) and hydrogen gas is pumped out on the cathodes side. The anode is forming chlorine from the sodium chloride, that is the transformed into sodium chlorate in the electrolyte. The cathode is splitting water.

Earlier electrolysis of chloride did problably also lead to formation of chlorate, but Hisinger and Berzelius were the first who recognized having prepared chlorate. A definite proof of the formation of chlorate through electrolysis of chloride solutions was given by Kolbe [11] in 1847. The first plant, producing chlorate under industrial conditions, was started by H. Gall and A. de Montlaur in 1886. [12]

1.4 Materials used in the electrochemical system

The electrochemical cell contains a very aggressive environment, pushing the standards of the materials in the system to the limit. Titanium is usually used as substrate of the anodes. The most well known chemical property of titanium is its excellent resistance to corrosion; capable of withstanding attacks by acids and moist chlorine in water. Titanium is very easily oxidised and it is this oxide that protects the rest of the metal from corrosion. For the coating of the anode, metal oxide from the platinum group metals is mainly used, such as ruthenium dioxide and iridium dioxide. Titanium is however vulnerable to hydrogen as it penetrates into the metal and causes embrittlement of the construction. Since the cathode is producing hydrogen gas from splitting water, titanium would be a bad choice for the cathode. Instead steel is the most commonly used as cathode material, and is kept from corrosion by cathodic protection. [1]

Chapter 2

Microscopy

THE INTENTION OF THIS CHAPTER is to provide information about the microscopy techniques used in this thesis. The basics of the three microscope techniques used; scanning electron microscope, transmission electron microscope and atomic force microscope, are described with instrument set-ups, sample preparation, measurement and characterisation techniques and some fundamental physics.

2.1 Electron interaction with specimen

When an electron beam hits a solid material, electrons (secondary electrons) as well as x-rays are released from the specimen. The electrons from the primary beam can be back-scattered (back-scattered electrons), diffracted or pass through the specimen as a transmitted beam (figure 2.1).

The number of secondary electrons emitted per second is high, and secondary electrons are therefore the most commonly used imaging signal in scanning electron microscopy (SEM). As the secondary electrons have low energy (less than 50 eV) these electrons usually come from the immediate surface of the specimen. Back-scattered electrons have lost some of their energy when colliding with the specimen and therefore contain information of the surface material. These electrons may also be used for imaging in SEM and gives an image that show relative atomic weights in the specimen. Back-scattered electrons comes from the near surface region (a fraction of a micrometer down in the specimen). The transmitted beam is used for imaging in transmission electron microscopy (TEM). The diffracted electrons contains information on

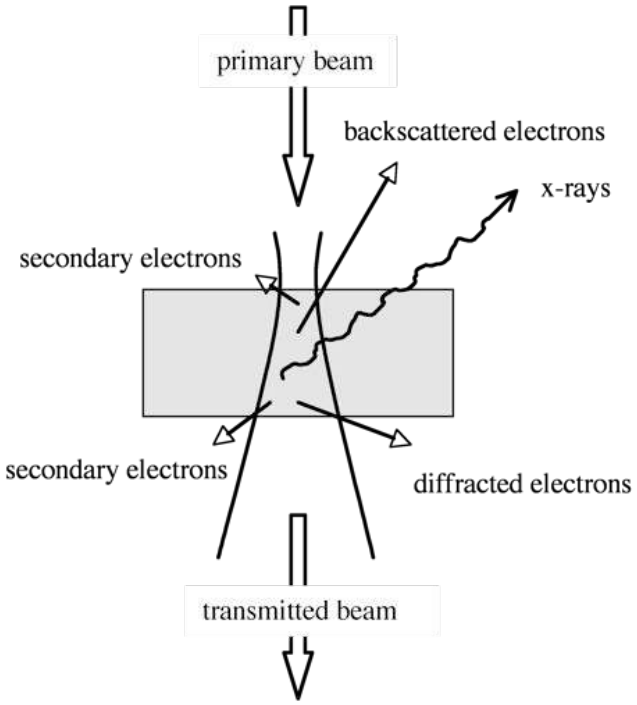

Figure 2.1: Schematic picture of electron interaction with specimen. The primary beam can be back-scattered, diffracted or pass through the specimen. On its way it releases secondary electrons and x-rays from the specimen.

crystal structure of the specimen and is used in TEM for electron diffraction and imaging.

The x-rays emitted from the specimen arise when excited atoms are relaxed. Excitation of atoms occur when the incoming electron knocks out one of the inner electrons. The x-rays contains information about the chemical composition of the sample and can be collected by a special x-ray detector and are common in both SEM and TEM. [13]

2.2 Scanning electron microscopy

Scanning electron microscopy (SEM) is primarily used to study surfaces. It can be used in the same ways as an optical microscope, or to get information about relative atomic weight in the sample. A SEM may also be used in analytical

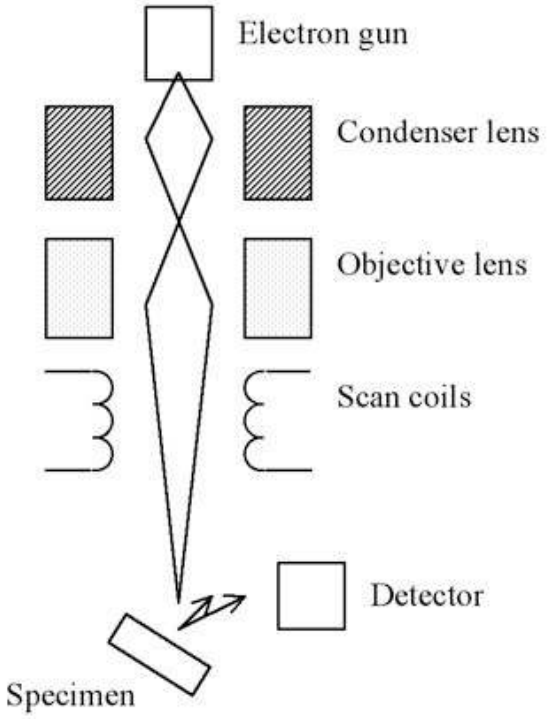

Figure 2.2: Schematic picture of SEM setup. The microscope contains an electron gun, some magnetic lenses and scanning coils and a detector. The electron gun produces the electron beam directed at the specimen. The back-scattered or secondary electrons emerging from the specimen is counted in the detector as the beam scans across the surface.

mode to detect x-rays (energy dispersive x-ray spectroscopy (EDS)). The resolution is approximately ten nanometers. Simply the SEM contains an electron gun, some magnetic lenses and scanning coils and a detector (figure 2.2). The electron gun produces the electrons and accelerates them (up to 20 kV in acceleration voltage), creating an electron beam directed at the specimen. As the electron beam is scanned across the specimen, the detector counts the number of scattered electrons from each point on the surface. The amplified current from the detector modulates the brightness of the spot on the picture. [13, 14]

As an electron gun requires vacuum, the sample can not contain gas or water. The sample surface also has to be electrically conductive, otherwise the electron beam will charge the sample and essentially decrease the quality of the image. If the sample is not conductive, a thin conductive layer of graphite or

gold can be deposited on the sample. The secondary electrons has too low energy to be detected, they therefore has to bee accelerated before entering the detector. A metal grid at a potential of several hundred volts surrounds the detector. It has two purposes; to prevent the high voltage of the detector to affect the primary beam and it attracts the secondary electrons and thus collects even those which were initially not moving towards the detector. The relative atomic weight information is collected in back-scatter mode. As a heavier atom scatter more electrons from the beam than a light one, a larger amount of back-scattered electrons will reach the detector when viewing a heavy atom, causing the corresponding pixel to be brighter.

SEM images were taken with a LEO 1450 EP scanning electron microscope.

2.3 Transmission electron microscopy

Transmission electron microscopy (TEM) uses the transmitted and diffracted electrons for imaging and analyse. It is usually larger than a SEM, the acceleration voltage in the electron gun is typically 200 kV, the sample is placed in the middle of the column with magnetic lenses both above and below it. The fluorescent imaging disc is placed at the bottom (figure 2.3).

There are two types of contrast mechanisms in TEM; mass-thickness contrast and diffraction contrast. One or both of them may contribute to the appearance on the TEM image. Mass-thicknees contrast means that a thick sample or a sample containing heavy atoms will transmit fewer primary electrons than a thin sample containing light atoms. Diffraction contrast occurs in crystalline samples, the diffracted electrons will not hit the imaging disc in imaging-mode. The diffraction will therefore cause the image to be darker. An image of a sample containing just one atom type, with uniform thickness could still show grain boundaries as a result of different grains diffracting with different diffraction values.

Unlike SEM that can analyse bulk samples, TEM requires very thin sample (less than 100 nm) which almost always means complicated sample preparation. The sample is normally place on a TEM-grid with a diameter of 3 mm. A standard TEM has a line resolution of 3 Å, to be able to se individual atoms a high-resolution TEM is needed. [15]

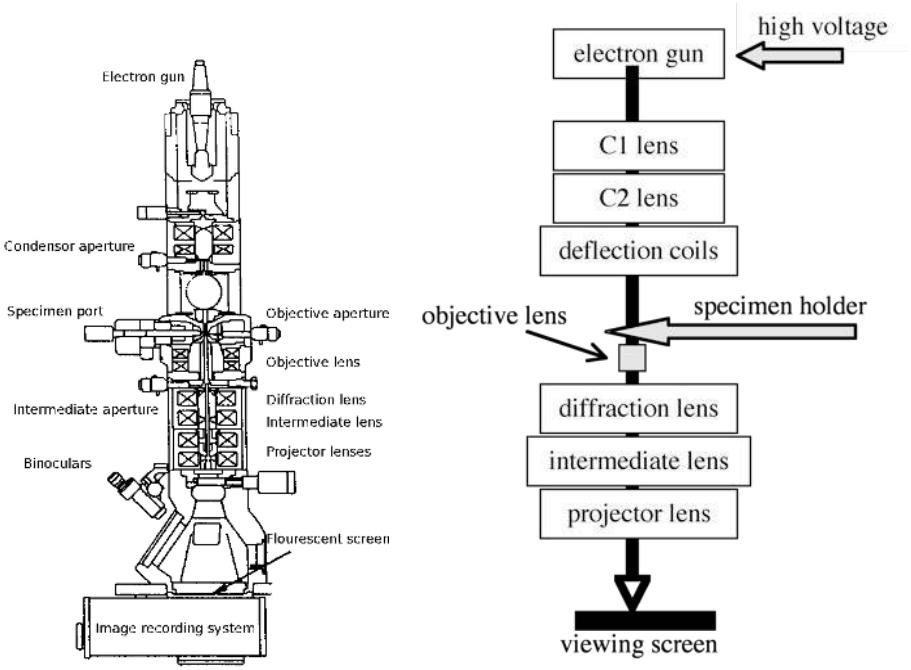

Figure 2.3: Schematic picture of TEM setup. The high voltage electron gun in the top of the column produces the beam. The sample is placed in the middle of the column with magnetic lenses both above and below it. The fluorescent imaging disc is placed at the bottom. Left image from wikipedia [49].

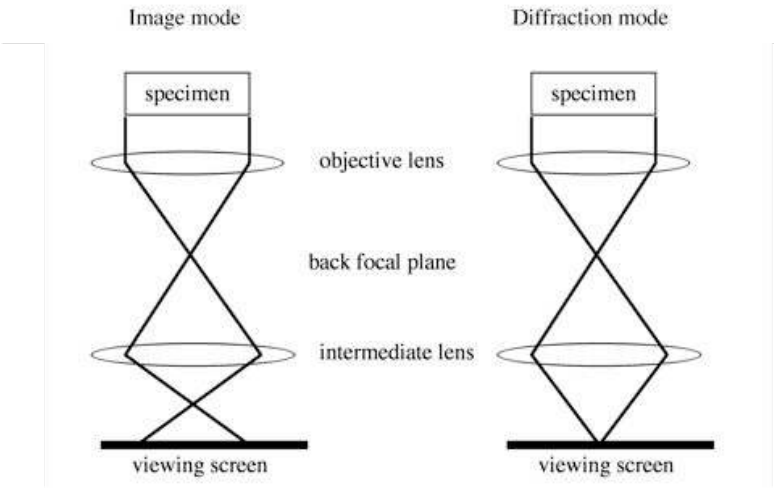

Figure 2.4: Schematic picture beam path in, left: imaging mode and right: diffraction mode in TEM. Electron diffraction is obtained by focusing the beam after penetrating the sample to a minimal spot.

Here a JEOL 2000FX TEM was used. The samples were prepared by scraping off the coating using a sharp knife and collecting the powder on TEM grids (Carbon grid 200 mesh), a simple and crude method that proved to be surprisingly successful. Cross section TEM sample preparation was done by Leica Mikrosysteme GmbH, Austria, using an ultramicrotome UC6.

2.3.1 Electron diffraction

Electron diffraction can be obtained by focusing the beam after penetrating the sample to a minimal spot. This very bright spot in the middle of the viewing disc is normally shaded do get a better picture of the surrounding diffraction pattern. Even when viewing a sample in image-mode, the diffraction pattern is created, but the diffracted electrons hits the walls of the column instead of the viewing disc and can therefore not be seen (figure 2.4). A diffraction pattern with spots evince that the material is crystalline. For each crystal direction, a new set of spots will appear in the pattern, rotated compared to the previous. A powder, or multi-crystalline sample, would therefore be represented by a pattern of circles. Just one set of spots in the diffraction pattern is evidence of

mono-crystallinity. The pattern itself is unique for each type of crystal structure and can be compared to a theoretical pattern found in a database. [13]

Extra spots in the diffraction pattern (small pattern around each spot in the first pattern) can appear with thick samples due to double diffraction. Extra spots can also appear as a result of superlattice reflection. [16]

2.4 Atomic force microscopy

Atomic force microscopy (AFM) is a technique to obtain the topography of a small sample. The AFM consists of a microscale cantilever with a sharp tip (probe) at its end that is used to sense the specimen surface. When the tip is brought close to a sample surface, forces between the tip and the sample lead to a deflection of the cantilever. Typically, the deflection is measured using a laser spot reflected from the top surface of the cantilever into a position sensitive photodiode (figure 2.5).

The AFM has several advantages over the SEM. Samples viewed by AFM do not require any special treatments (such as metal/carbon coatings). While an electron microscope needs vacuum environment for proper operation, most AFM modes can work perfectly well in ambient air or even a liquid environment. A disadvantage of AFM compared with the SEM is the image size. The SEM can image an area on the order of millimetres by millimetres. The AFM can only image a maximum scanning area of around 150 by 150 micrometres. Another inconvenience is that an incorrect choice of tip for the required resolution can lead to image artifacts. The AFM could also not scan images as fast as an SEM, requiring several minutes for a typical scan.

The first AFM mode invented was contact mode. The tip is dragged along the surface and the static tip deflection is used as a feedback signal. The problem with this technique is that a soft sample could be damaged by the tip, a very hard sample on the other hand will break the tip. Non-contact modes were therefore invented, using the interaction forces between the tip and the sample to regulate the frequency or amplitude of the oscillating tip when it closes in on the sample surface. [17]

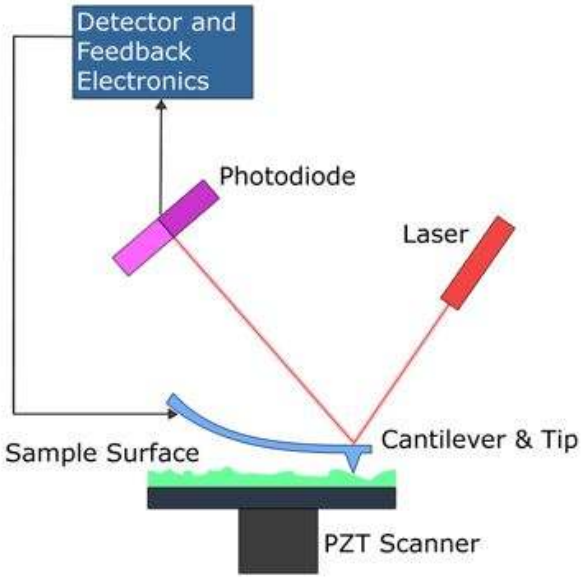

Figure 2.5: Schematic picture of AFM setup. The AFM consists of a microscale cantilever with a sharp tip. When the tip is brought close to a sample surface, forces between the tip and the sample lead to a deflection of the cantilever. The deflection is measured using a laser spot reflected from the top surface of the cantilever into a position sensitive photodiode. Image from Wikipedia [49]

Here, a Digital Instruments Dimension 3100 AFM was used, in tapping mode. In tapping mode the cantilever is driven to oscillate up and down at near its resonance frequency by a small piezoelectric element mounted in the AFM tip holder. The amplitude of this oscillation is typically 20 to 100 nm. The amplitude is reduced due to a short contact with the sample during each cycle.

Chapter 3

Other characterisation methods

IN THIS CHAPTER some other characterisation techniques used in this thesis are described briefly. The intention is to give a quick overview of the different techniques, the interested reader is directed to the works of reference.

3.1 Porosimetry

Porosimetry is an analytical technique used to analyse a porous material, to determine pore diameter, total pore volume, surface area, etc. The technique is to push a non-wetting liquid (often mercury) into the material using high pressure. The pore size can be calculated using Washburn's equation [18], based on the external pressure needed to force the liquid into a pore against the force of the liquid's surface tension. A variation of the technique is to use liquid nitrogen instead of mercury as the nitrogen can penetrate deeper into the material and thus measure smaller pores (less than 6 nm in diameter). The calculations are in this case based on adsorption and desorption isotherms of the nitrogen using the Barrett, Joyner, Halenda model [19]. Knowing the pore size distribution, the surface area of the sample can be calculated using the BET function [20]. Assuming the grains to be spheres, the average grain diameter can be calculated from the total surface area.

Gas porosimetry and Bruanauer Emmet Teller (BET) measurements were made using a Micromeritics, ASAP 2010 porosimeter. Nitrogen adsorption data was analyzed using a Barrett, Joyner and Halenda model. Prior to measurements the samples were degassed at 100 °C.

3.2 X-ray diffraction

X-ray diffraction is a technique of obtaining the crystal structure of a sample, depending on at which angles in the diffractogram the peaks appear. It can also be used to estimate the average crystal size as it is a volume averaging technique, by analysing the width of the peaks, the larger the crystallites, the narrower the peak. The Scherrer equation was used to estimate the average crystal size:

$$L = \frac{K\lambda}{\beta \, cos\theta}; \tag{3.1}$$

where L is the mean size of the crystallites in the sample, β is the width of the peak (at half maximum intensity) in the diffraction profile (measured in radians) and K a constant approximately equal to unity [21].

X-ray diffraction was done with the grazing incidence technique on a Siemens D5000 diffractometer (Cu $K_\alpha, \lambda = 1.5406$ Å). A Sol-X detector scanned between $24 - 60\,^\circ$ in 2θ with the angle of incidence of $0.5\,^\circ$.

3.3 Cyclic voltammetry

The voltammetric charge was evaluated from cyclic voltammograms. Cyclic voltammetry is a type of potentiodynamic electrochemical measurement (this means varying the potential and measuring the current). In cyclic voltammetry the working electrode potential is ramped linearly versus time, when the potential reaches the set point the potential ramp is inverted, creating a cycle. This is repeated multiple times during an experiment. The voltammetric charge is obtained by integrating the current with respect to time and is an estimate of the active surface area of the electrode. [22]

Voltammetric charge, q*, was evaluated from cyclic voltammograms measured in deaerated 1M NaOH at 25 °C. Circular electrode samples, 1 cm^2, were used. A platinum mesh served as the counter electrode and the reference electrode was a saturated calomel electrode (SCE) from Radiometer Copenhagen. The voltammograms were measured between -0.8 and $+0.2$ V vs. SCE with a sweep rate of 20 mV/s.

3.4 Spin-coating

The principle of spin coating is that a circular substrate is placed on a vaccum chuck that can rotate in high speed (typically 6000 rpm). A liquid solution is then dripped onto the substrate while it spins, causing the liquid to form a thin layer of very homogenous thickness on the substrate while the redundant solution is spinned off.

Thin film electrodes were made by spin coating silicon wafers with ruthenium-titanium dioxide coating. To help the adherence of the coating, a thin layer of metallic titanium was pre-deposited on the wafer. Silicon wafers (4″) where cleaned in hydrofloric acid (1%) and a 100 nm layer of metallic titanium was deposited on the wafer. A few drops of coating solution ($RuCl_3$ and $TiCl_4$ dissolved in n-butanol) was placed on top of the titanium and spinned out to form a even layer. The wafer was then dried on a hot-plate for 1 minute and heat-treated in air in 450 °C for 10 minutes. Resulting in an approximately 200 nm thick layer of $Ru_{0.3}Ti_{0.7}O_2$.

3.5 Ellipsometry

Ellipsometry is an optical technique for the investigation of the dielectric properties of thin films. It is commonly used to characterize film thickness ranging from a few angstroms to several micrometers with excellent accuracy. The method is non-destructive and self-normalising. There are two types of ellipsometry; single-wavelength ellipsometry and spectroscopic ellipsometry. Single-wavelength ellipsometry uses a single wavelength light source, while spectroscopic ellipsometry uses broad band light sources, which cover a certain spectral range in the infrared, visible or ultraviolet spectral region. If the dielectric function of the material is known, single-wavelength ellipsometry is a fast and non-distructive way of measuring the film thickness. The sample must be composed of a small number of discrete, well-defined layers that are optically homogeneous and isotropic. If the dielectric function of the material is not known, spectroscopic ellipsometry can be used to obtain it. [23, 24]

Spectroscopic ellipsometry measures the polarisation change upon reflection on a sample. The polarisation of the beam is changed due to refraction index mismatch of the sample against its surrounding environment, e.g. air. The complex refractives are denoted r_p and r_s, and the ellipsometric parameters Ψ and Δ are calculated from the ratio of r_p and r_s

$$\rho = \frac{r_p}{r_s} = \tan(\Psi)e^{i\Delta}. \tag{3.2}$$

Thus, $tan\ \Psi$ describes the amplitude change upon reflection, and Δ the phase change. [23]

The measurements were performed using an extended Sentech SE850 spectroscopic ellipsometer, capable of covering a spectral range between 0.5 and 5.5 eV. In the shown result, only the visible range was measured, using a Xe discharge lamp as light source and a grating spectrometer with a photo-diod array detector for data recording.

Chapter 4

Summary of papers

In this chapter the two appended papers; Nanoscaled characterisation of DSA® and Dependence on production parameters, are summarised. A section on cracked-mud structure presents some backgroud results and a section on thin film electrodes presents a first step towards patterning of electrodes.

4.1 Cracked mud structure

TODAY, THE ANODES ARE PRODUCED by painting a titanium plate with an aqueous salt solution containing ruthenium- and titanium chloride. The chloride-solution coated anode is heat-treated twice; first at moderate temperature to drive out excess solvent, next at higher temperature to calcinate the coating. As the metal substrate is expanded in the heat treatment much more than the coating, tensions are built in causing the coating to crack. This is called the ”cracked-mud” structure (figure 4.1) and was first described by Pizzini *et al.* [25] in 1972. The size of the plaquettes depend on, for example, the solvent of the coating solution.

The cracks as observed in cross section scanning electron microscopy (SEM) pass through several layers in the coating. The separate layers can be seen as altering bright (ruthenium-rich) and dark (titanium-rich) lines. A heavier atom scatter the electrons from the beam more than a light one, in SEM causing the corresponding pixel to be brighter. In cross section transmission electron microscopy (TEM) the structure of each layer is visible, with a dark ruthenium-rich core flanked by bright titanium-rich stripes on both sides (figure 4.2). In

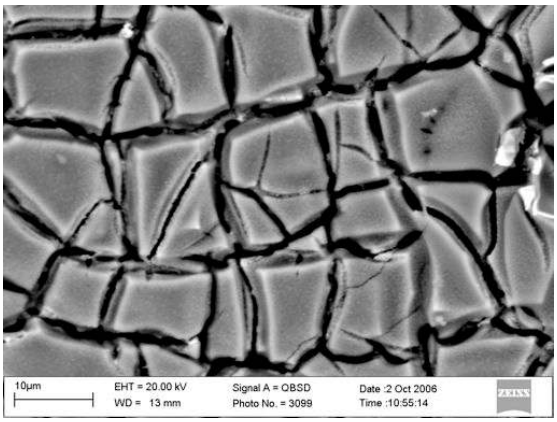

Figure 4.1: SEM image of a DSA® coating. As the metal substrate is expanded in the heat treatment much more than the coating, tensions are built in causing the coating to crack. This is called the ”cracked-mud” structure.

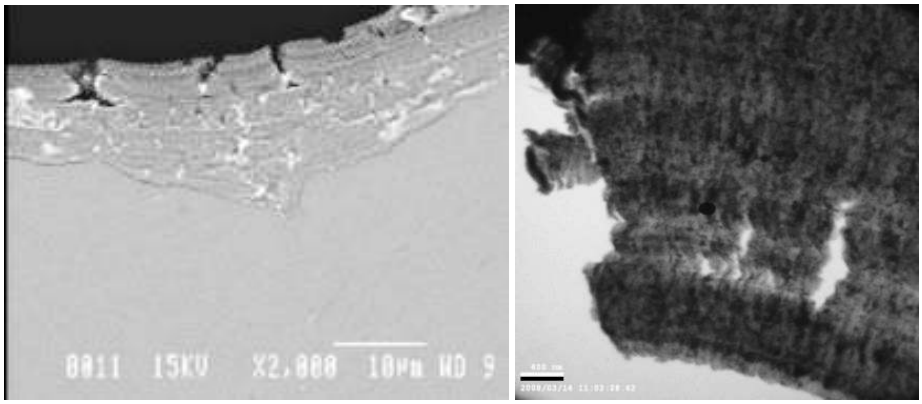

Figure 4.2: Left: SEM cross section image of DSA® coating. The cracks is seen to pass several microns down the coating. A thick coating is more severely cracked than a thin one. The separate layers are visible as altering dark (titanium-rich) and bright (ruthenium-rich) lines. Right: TEM cross section image of coating. The structure of each layer can be seen, with a dark ruthenium-rich core flanked by brighter titanium-rich stripes on both sides.

TEM, the scattered electrons will not hit the imaging disc, a heavy atom will therefore be represented by a dark pixel.

4.2 Nanoscaled characterisation of DSA® – Paper I

ONE MIGHT NAIVELY BELIEVE that the large catalytic area of the DSA® is due to the cracks visible in figure 4.1 and 4.2. However, the high increase in surface area cannot be explained by the cracked-mud structure alone, even though the cracks probably have a significant role in mass-transport. A better suggestion is that the the coating is nano-porous. To directly measure the surface area is a difficult task [26] and instead in-situ electrochemical methods have mainly been used [27]. In paper I, a combination of ex-situ methods such as atomic force microscopy, transmission electron microcopy and gas porosimetry is used to estimate the effective surface area and to reveal the microstructure of the coating.

Atomic force microscopy (AFM) imaging on top of the plaquettes show a rough surface on the nanoscale. TEM show that this is not just a surface phenomenon, but the whole coating is built up of $20 - 30$ nm sized grains, and the bumps in the AFM images are the top of the grains visible in the TEM images (figure 4.3).

The pore diameter can be estimated using a simple model. For a sphere diameter of 20 nm the corresponding pore diameter will be 8 nm, and for a 30 nm sphere the pore will be 13 nm.

To check this, the pore diameter was measured by gas porosimetry and found to be between 10 and 13 nm. Thus the microscopy and porosity measurements are consistent.

The grains visible in the TEM image do not necessarily have to be crystallites, therefore this was investigated using electron diffraction. The coating consists of two oxides, ruthenium dioxide (RuO_2) and titanium dioxide (TiO_2). TiO_2 crystallizes in rutile and anatase structure and RuO_2 crystallises in rutile. With the same crystalline structure of the two oxides, the ruthenium atoms should be able to replace titanium atoms in the rutile structure in a mixed oxide [2]. It is interesting to see whether a grain consists of one or multiple crystallites. When studying the grains one by one with electron diffraction in TEM, the rutile mono-crystallinity of the grains can be seen.

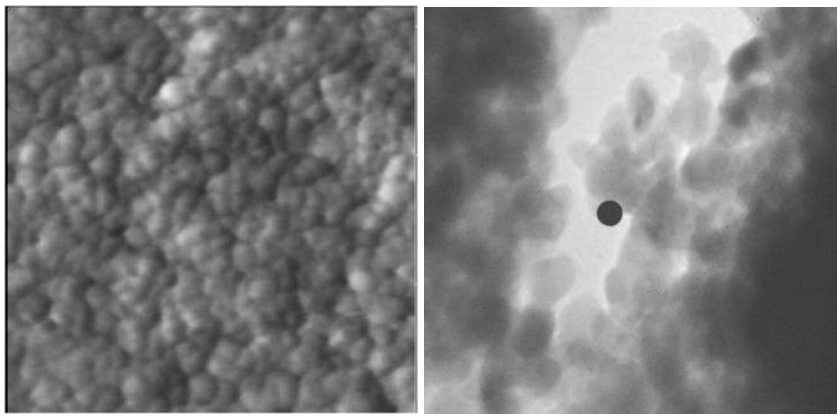

Figure 4.3: Left: AFM image of the top of a plaquette. 20 nm wide grains are closely packed together all over the plaquette top surface. The grayscale is 6 nm. Right: TEM image of coating scraped of the substrate and placed on a TEM grid. The whole coating consists of $20 - 30$ nm grains. (The black circle in the centre is a non-fluorescent spot on the imaging disc.)

4.3 Dependency on process parameters – Paper II

A COATING CONTAINING small grains logically has a larger surface than a coating containing large grains. A method to control the grain size would thus be a way to control the electrode efficiency. By minor changes in the process parameters, the crystallising conditions will change and affect the size of the created crystallites. The preparation parameters that is easy to change without developing a new production recipe is; precursor and solvent of the coating solution, drying and calcination temperature and duration. In paper II a study is described on the effects on ruthenium dioxide prepared with varying calcination temperature and changing the precursor to ruthenium nitrosyl nitrate instead of the more commonly used chloride salt, combining physical and electrochemical measurement techniques.

TEM images showed coating grains of rather uniform size distribution for each sample. The grains are smaller for lower calcination temperatures. It is difficult to get a representative quantitative estimate of the crystallite size using TEM, due to the limited sampling volume.XRD, being a volume averaging technique, could provide more accurate estimates.

From the x-ray diffractograms (figure 4.4a) the crystallite size in the sample can be estimated by the Scherrer equation (equation 2.1) [21]. The estimation is

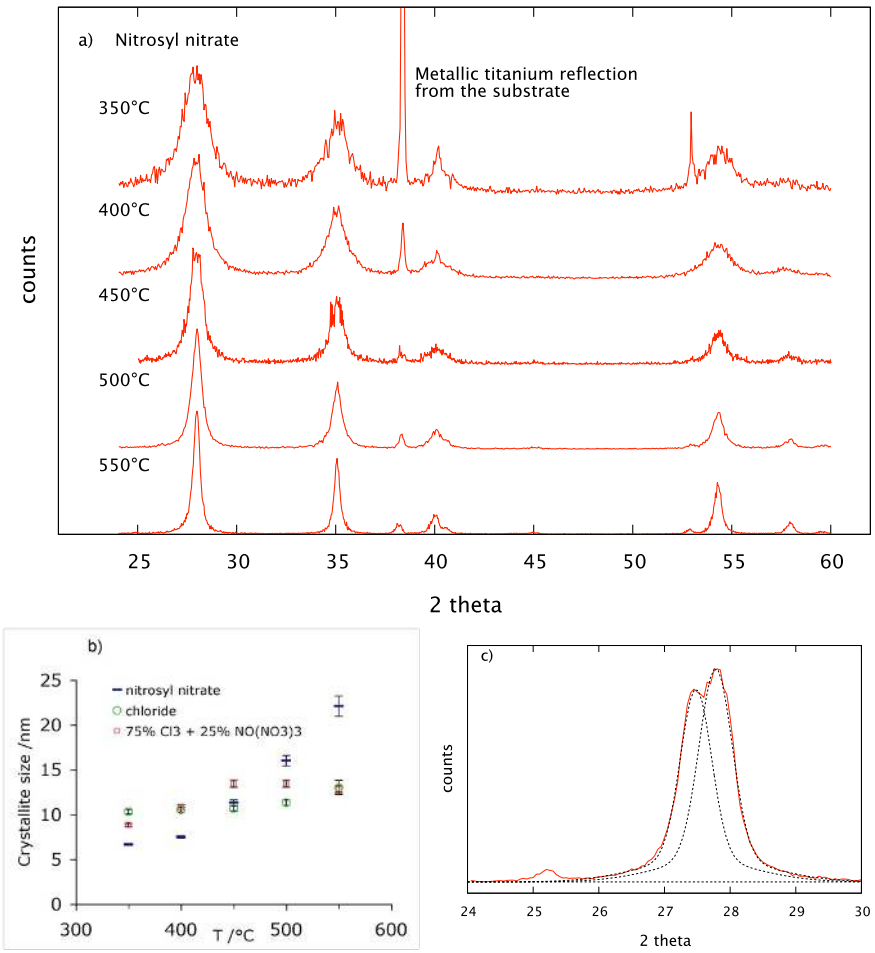

Figure 4.4: a) Measured diffraction patterns, illustration the varying peak width. Curves are offset for clarity. b) The crystallite size in the sample calculated from the breadth of the diffraction peak, using the Scherrer equation. c) The growth of titanium oxide during annealing is visible in the ruthenium dioxide prepared from chloride and calcinated at 550 °C, as a double peak at $2\theta = 27\,^{\circ}$, representing the rutile phase of titanium and ruthenium dioxide, respectively, and at the titanium dioxide anatase phase peak at $2\theta = 25\,^{\circ}$.

valid under the assumption that all line broadening is due to finite crystallite sizes. As shown in figure 4.4b the crystallite size increases with increasing calcination temperature. The trend was clearer for the RuO_2 samples prepared from ruthenium nitrosyl nitrate, with a four-fold increase of crystallite size while for the RuO_2 samples prepared from ruthenium chloride the trend was less profound. Nitrosyl nitrate decomposes at a lower temperature than chloride [28] and could be the reason why the temperature dependence on crystallite size is effective at a lower temperature.

Using XRD, a growth of titanium oxide was found in all samples calcinated at 550 °C and in samples prepared from chloride calcinated at 450 °C and above. The TiO_2 signal was generally very weak compared to the RuO_2 signal, with the exception of the chloride 550 °C sample (figure 4.4c). It showed clearly a double peak at approximately $2\theta = 27°$, representing the rutile phase of titanium and ruthenium dioxide, respectively, and a small titanium dioxide anatase peak at $2\theta = 25°$. Since in this case the coating consists of pure RuO_2 the only available source of titanium is the substrate. When instead using mixed oxides of ruthenium and titanium the same double rutile peak sometimes occur in the x-ray diffractograms, as a result of phase separation during heat-treatment.

The voltammetric charge (q*) decreased with increasing calcination temperature. It was also lower for electrodes prepared from chloride than for electrodes prepared from nitrosyl nitrate, but the precursor dependence decreased with increasing temperature. At low temperatures the precursor had a large impact on the voltammetric charge; more nitrosyl nitrate gave a higher voltammetric charge. At high temperatures there was almost no precursor dependence at all. Since the voltammetric charge is proportional to the active area of the electrode [29], and the grain size has a direct influence on the total area, a sample with small grains and large total area would have a larger active area and therefore higher voltammetric charge.

From the porosimetry, the BET surface area can be obtained. The BET surface area measurement gave an approximate value of the total surface area of the sample. From BET surface area measurement the mean diameter of the grains can be estimated under the assumption that the coating consists of loosely packed spherical grains with uniform size distribution.

The so-estimated grain sizes can becompared with the crystallite sizes estimated from XRD measurements. The XRD and BET agree qualitatively is the sense that samples prepared from $RuCl_3$ display grain sizes almost indepen-

dent of preparation temperature, while $RuNO(NO_3)_3$ yields highly temperature dependent grain diameters. (This is further in qualitative agreement with the voltametric charge.However, quantitatively, there is about a one order-of-magnitude discrepancy between the sizes estimated from porosimetry and diffraction data. The explanation is most likely that the crystallite grains are not loosely packed. They are rather sintered or clustered together in such a way that only a fraction of the boundary surface of the crystallites is accessible for the gaseous probe of the porosimetry. An additional, interesting discrepancy is that the temperature trends of the grain sizes determined from XRD or porosimetry have a crossing somewhere between the highest and the lowest temperature (i.e. at low temperature, chloride results in larger diameters than nitrosyl nitrate, but at high temperature this is reversed). This cannot be observed in the voltammetry data,where the high temperature yields the smallest active surface independent of precursor. This means that gas porosimetry and cyclic voltammetry do not probe exactly the same surface.

In conclusion, ruthenium nitrosyl nitrate, calcinated at a low temperature ($350-400\,^{\circ}C$) resulted in ruthenium dioxide particles that were rather small ($5-10$ nm). Because of the small particles in the coating, such an electrode had a large total area and high voltammetric charge. The same precursor calcinated at a high temperature ($500-550\,^{\circ}C$) showed instead an opposite trend with large particles ($20-30$ nm), small total area, and low voltammetric charge. Ruthenium chloride calcinated at any temperature in the range $350-550\,^{\circ}C$ showed ruthenium dioxide particles of about 12 nm, which is similar to that of ruthenium nitrosyl nitrate calcinated at $450\,^{\circ}C$.

4.4 Thin films – toward nanopatterned electrodes

IN ORDER TO BE ABLE TO ETCH a pattern into the coating of an electrode, using for example nanoimprint lithography (section 5.2), the electrode must be very smooth to get the (polymer)-mask to stick to it. The substrate must be flat and there must not be any cracks in the coating. Electrodes were therefore made by spin coating silicon wafers to form an even, almost perfectly flat electrode. These electrodes were characterised by SEM, AFM and ellipsometry.

The thin coating layer looks a bit worm-eaten in the AFM image. The grains can yet be seen as 30 nm wide dots in the image (figure 4.5). Cross-section SEM reveals the thin coating film, with an even thickness on the flat substrate (figure 4.6). The 100 nm of metallic titanium and the about 200 nm thick coating

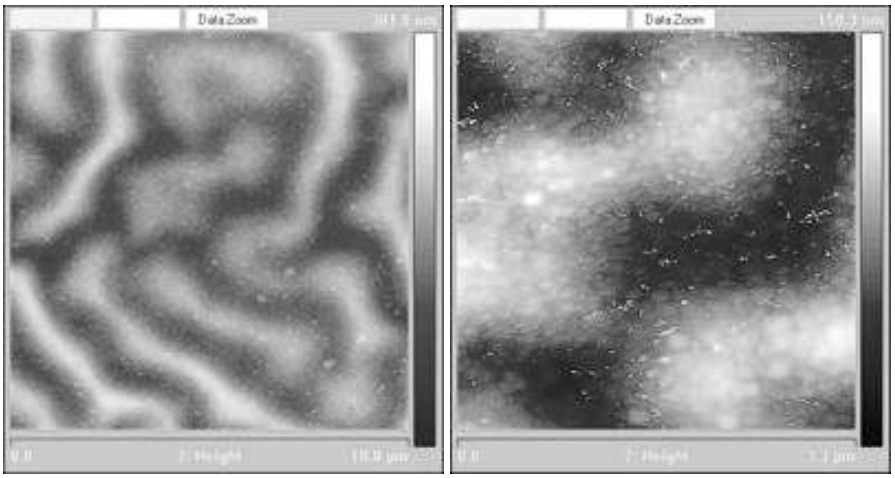

Figure 4.5: AFM images of thin film $Ru_{0.3}Ti_{0.7}O_2$ coating on silicon. The thin coating layer looks a bit worm-eaten, the grains can still be seen as 30 nm wide dots. The "worms" are approximately 100 nm high.

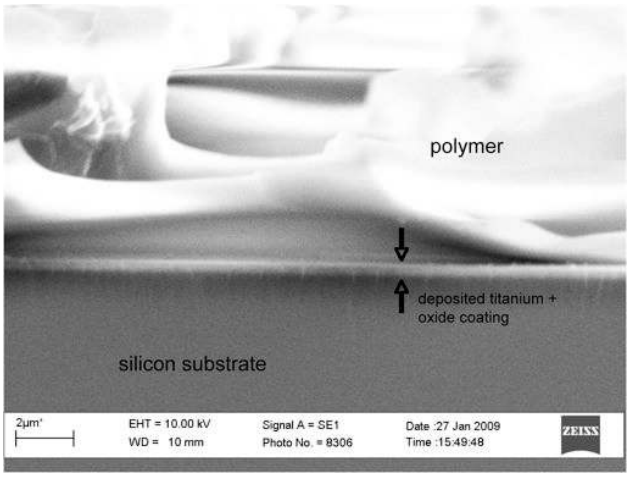

Figure 4.6: Cross-section SEM image of spin-coated electrode with imprinted polymer on top (see section 5.2). The polymer pattern is damaged due to sample preparation. The $Ru_{0.3}Ti_{0.7}O_2$ coating and metallic titanium layer is visible as a thin bright line in the centre of the image. The silicon substrate is beneath.

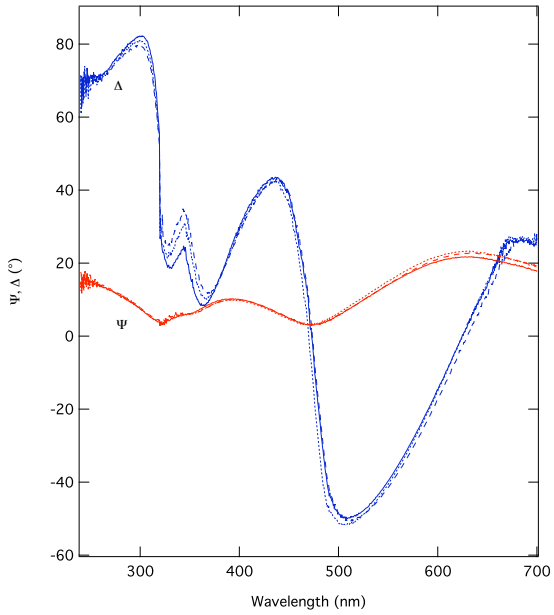

Figure 4.7: Psi (Ψ) and delta (Δ) values as a function of wavelength for three different spots on the same thin film electrode. The good analogy between the spots evince that the sample is homogeneous and isotropic. It is also an evidence of the uniform film thickness in the sample.

film is seen as a bright line in the centre of the image. The ”worm-eaten”-pattern can be seen at the top of the coating layer, at least in the very left of the image. An imprinted polymer has been placed on top of the thin film electrode as preparation for etching, it however got damaged in cross section sample preparation and looks a bit like a bright cloud in the upper half of the image.

To be able to directly derive the bulk dielectric function of the material from the ellipsometrically measured reflectance ratio, the sample besides homogeneity and isotropicallity, also has to have an uppermost layer that is much thicker than the penetration depth of the light. [23]

Figure 4.7 show the Ψ and Δ as a function of wavelength for three different spots on the same thin film electrode. The good analogy evince that the sample is homogeneous and isotropic. Comparison between different samples to obtain the dielectric function of the material $Ru_{0.3}Ti_{0.7}O_2$ is difficult due to the thin oxide layers of the samples.

Chapter 5

Future work

THE SUCCESS OF THE DSA® depends on the large catalytic area of the coating, a coating that is shown in this work to be nano-crystalline. A logical step to further improve the anode would be to mechanically make the reachable surface area even larger. The electrolyte of the production cell does probably not penetrate through the entire coating volume. A patterned coating at the nanoscale would therefore increase the reachable coating volume. Another way to increase the area might be to grow a "forest" of nanowires. These ideas are discussed in this chapter.

5.1 Nanowire growth

Resarech on one-dimensional structures, such as nanowires, have been done for about 20 years. Still they attract a great scientific interest. Wires, whiskers, rods and tubes have been fabricated from of variety of metals, semiconductors and oxides. Functional 1D structures have got a lot of attention because of their unique applications [30], such as building blocks for nanoelectronics and reinforcement in concrete or plastic. Nanowires also exists in nature, for example on the feet of a gecko, which is using van der Waal forces to stick to the wall while climbing [31]. Nanowires normally consist of just one, almost perfect crystal, giving superior mechanical properties. A carbon nanotube for example has about 10 times higher Young's modulus and more than 20 times the tensile strength of steel [32]. A forest of nanowires theoretically has a surface area that could be several hundreds times larger than the flat surface. Since ruthenium dioxide is the material active in the catalytic process, wires made

out of this material would work as an electrode, growing them like a forest would hence create an electrode with large surface area. Some attempts of growing ruthenium dioxide nanowires were made, however without success.

Four different sets of nanowire synthesis experiments was performed. In the first set-up, oxygen was used as pushing gas, and the pump kept the pressure inside the tub at 0.5 mbar. At this point ruthenium was moved from the source to the substrate but no structures were notised (figure 5.1a). In the second set-up the pressure was raised to 2 mbar as in the report of Liu *et al.* [33]. This created large, clearly rutile, ruthenium dioxide structures on the substrate, more microstructures than nanowires (figure 5.1b). In the third trial, the inlet valve was closed and the pump was not used. The tube was just sealed at atmospheric pressure, trapping air inside as Backman *et al.* [34] suggest. In this case nanowires were created on the substrate (figure 5.1c), but they turned out to be amorphous rather than crystalline (figure 5.1d), decorated with particles with low melting point (figure 5.1e), since they were easily melted by the electron beam in the microscope. The wires were suggested to be of silicon dioxide as it is an amorphous material and gold nano-particles placed on silicon in high temperature is known to create silicon whiskers that are then oxidised to silicon dioxide. An alloy of silicon and gold in the right propotions has a meltingpoint just above 650 °C. The particles are therefore suggested to be of gold-silicon alloy. Previously titanium was used as substrate, resulting in titania wires (figure 5.1f). Silicon was instead used as substrate to prevent this as most references use silicon substrates. In the last set-up, the silicon substrate was replaced by a titanium substrate, precoated with ruthenium dioxide. This time no stuctures were found on the substrate besides the cracked-mud of the precoat (figure 5.1g). What this show is that we are able to grow quite large single crystals of rutile rutehnium dioxide.

5.2 Nanoimprint lithography

Nanoimprint lithography is a fast and economical way to replicate a pattern. It was invented about 15 years ago [35]. The principles of the technique is that a UV-hardening polymer is spinned onto a silicon wafer to form an even layer. A pattern is mechanically printed into the soft polymer using a stamp, the polymer is then hardened by illumination of UV-light. When the stamp is removed it can be used to print another wafer with the same pattern, over and over again. The imprinted polymer can be used as it is or be used as a mask for further etching in what is underneath the polymer (figure 5.2). [36]

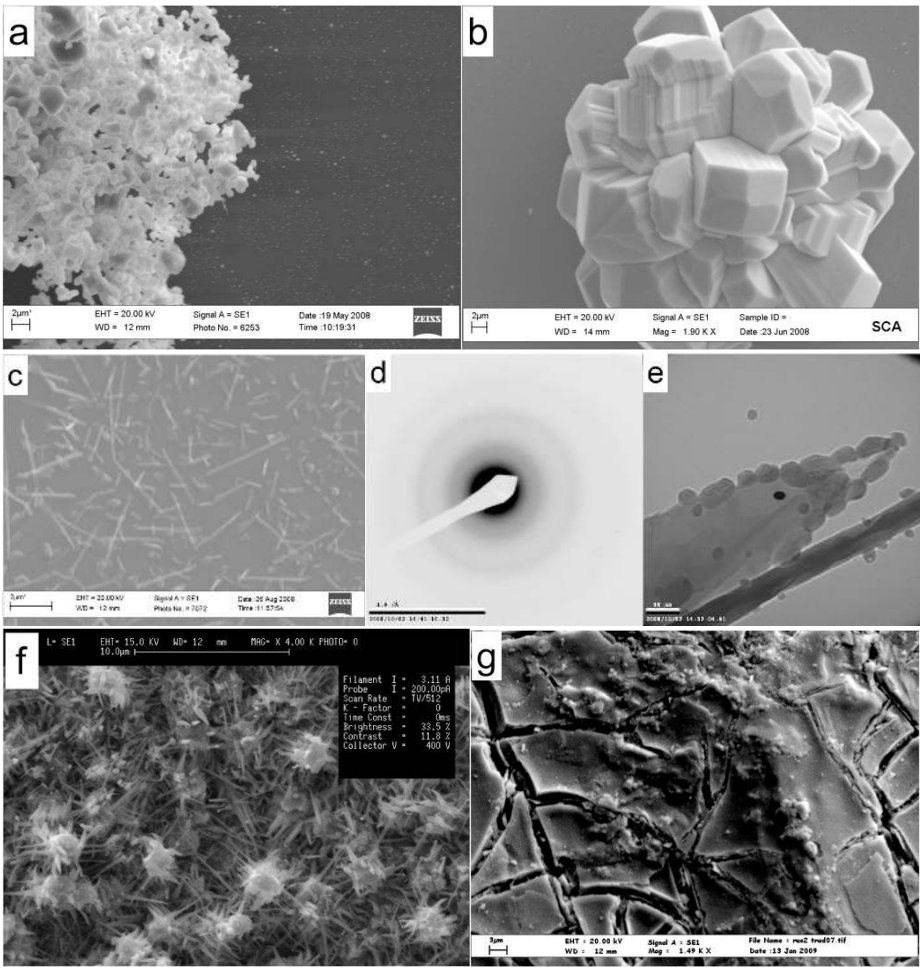

Figure 5.1: Different stages in the development of nanowires. **a)** Ruthenium dioxide "porrige" on silicon substrate, **b)** ruthenium dioxide obelisque on silicon, **c)** SEM images of silicon dioxide whiskers, **d)** electron diffraction of silicon dioxide whisker, showing it to be amorphous, **e)** TEM image of silicon dioxide whisker, the whisker is decorated with particles of silicon-gold alloy, **f)** titania wires spontaneously grown on titanium substrate and **g)** ruthenium dioxide flakes on titanium precoated with ruthenium dioxide, the cracked-mud structure of the precoat is visible.

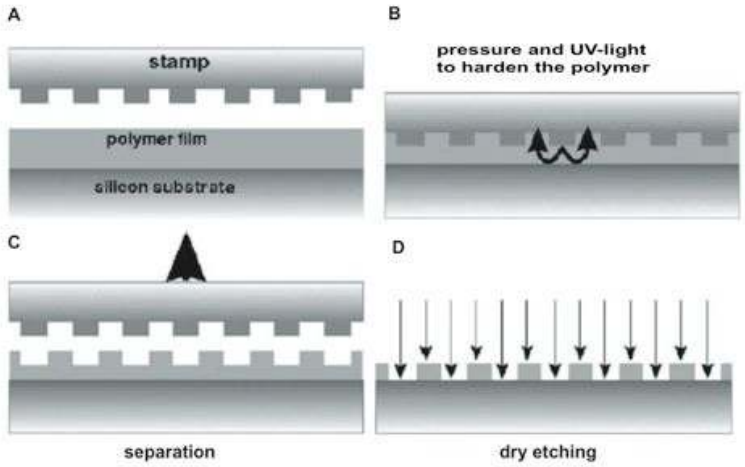

Figure 5.2: Principle of nanoimprint lithography. **A** A UV- or temperature hardening polymer is spinned onto a silicon substrate, **B** a pattern is mechanically printed into the polymer, and the polymer is hardened, **C** the stamp is separated from the imprint, **D** the imprint is etched to erase the residual layer. Image from Sotomayor *et al.* [36].

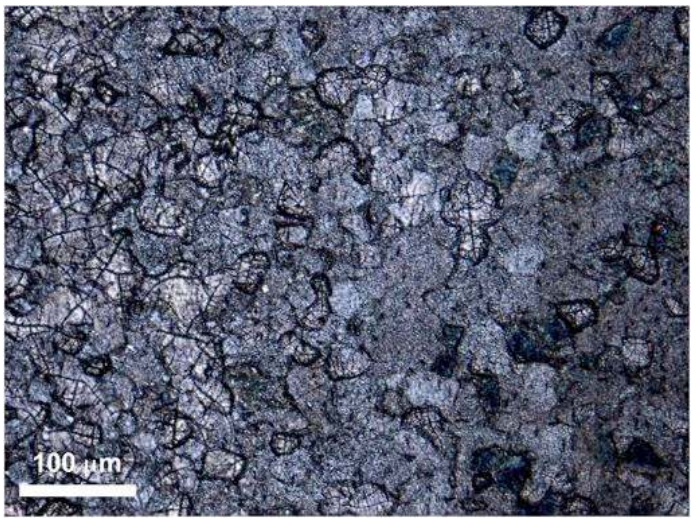

Figure 5.3: Micrograph of sol-gel coating. The plaquettes are a bit larger than coatings made from aqueous solutions. The bluish colour is a result of polarisation in the microscope.

5.3 Sol-gel based coating solution

An attempt to make a patterned electrode was made using a sol-gel coating. A sol is a dispersion of a solid in a liquid, or of a solid in a solid. A gel is a semirigid mass of a lyophilic (– solvent attracting) sol in which all the dispersion medium has penetrated the sol particles [37]. The idea was to make an electrode with a coating suitable for mechanical printing. A ruthenium chloride containing gel should be used as coating and a pattern should be printed into the gel before hardening. The electrode should then be heat-treated to oxidise the ruthenium chloride to ruthenium oxide and burn off the organic parts, leaving a ruthenium oxide layer in the shape of the pattern.

After drying, the sol-gel coating looks completely black and glossy. After heat-treatment the normal dark grey colour appears and the coating is cracked (figure 5.3). It might be possible to print a pattern in the gel coating before drying. There are however some problems. The coating gel consists of a very large volume of organic material compared to the total volume. Ideally the organic part burns away, leaving a thin layer of RuO_2 on the substrate. This means that many layers is required to reach the wanted ruthenium load. This also means that whatever pattern printed in the undried gel most likely will be lost during the process.

5.4 Discussion

The nanowire technique is promising, as a nanowire forest theoretically would increase the surface area several hundred times. Growing nanowires on a pre-coated electrode is however not a good idea. As the substrate already is ruthenium dioxide in rutile there is no benefit in nanowire construction compared to simple deposition on the surface. A gel-based coating solution could be successful method of producing electrodes [38], the profits with such an electrode have not been investigated here though.

Some ideas that came up during the project, but was not tested, is surfactants in the coating forming micelles that can be burnt away in calcination [39]. Giving rise to deep pores assisting the mass-transport and access of the electrolyte to the deep layers of the coating. Another idea on the same theme is to fill the coating with pieces or particles of a material that is corroded away during use of the electrode gradually giving access to the deeper layers of the coating.

Chapter 6

Conclusion

THE WORK HERE SHOWS that the anode coating consists of faceted monocrystalline grains of $20 - 30$ nm in diameter. The superior catalytic properties of the DSA® is due to the large electrocatalytic area of the coating. The grains increase the surface area by approximately three times for every layer of grains. A normal coating of 10 μm thus have about 300 layers of grains, increasing the total area by about thousand times.

The size of the grains can be controlled by the manufacturing parameters. A smaller grain results in a larger surface area for the same volume of coating in total. When using ruthenium nitrosyl nitrate as precursor for the ruthenium dioxide in the coating a lower calcination temperature creates smaller grains. At 350 °C the average grain diameter is 6 nm giving a total area that is five times larger than the standard coating. A too low calcination temperature will however not fully oxidise the coating leaving residual precursor in the coating, which is not favourable.

A forest of nanowires would theoretically increase the surface area by several hundred times compared to the flat surface. Nanowires are, thanks to their minimal size and perfect crystal structure, very stable and robust. An electrode covered by a forest of nanowires is promising as it could have very large surface area, easy access and mass-transport channels for the electrolyte and still be very stable. Patterning, using for example nanoimprint is another way to increase the area. Therefore, these are potentials for creating totally different type of electrodes, manufactured in other ways than the 1965 recipe.

Bibliography

[1] S. Trasatti, G. Buzzanca *Ruthenium dioxide: a new interesting electrode material. Solid state structure and electrochemical behaviour* J. Electroanal. Chem. **29** (1971) App. 1.

[2] S. Trasatti *Electrocatalysis: understanding the success of DSA®* Electrochim. Acta **45** (2000) 2377.

[3] Permascand website: www.permascand.se

[4] H.B. Beer, British Patent 1,147,442; 1965

[5] P.C.S. Hayfield *Development of the Noble Metal/Oxide Coated Titanium Electrode, part I* Platinum Metals Rev. **42** (1) (1998) 27.

[6] P.C.S. Hayfield *Development of the Noble Metal/Oxide Coated Titanium Electrode, part II* Platinum Metals Rev. **42** (2) (1998) 46.

[7] P.C.S. Hayfield *Development of the Noble Metal/Oxide Coated Titanium Electrode, part III* Platinum Metals Rev. **42** (3) (1998) 116.

[8] A. Cornell *Electrode Reactions in the Chlorate Process* (2002) Royal Institute of Technology, Stockholm, Sweden

[9] G. Lindbergh *The Effect of Chromate Addition on Chlorate Cathodes* (1990) Royal Institute of Technology, Stockholm, Sweden

[10] W. Hisinger, J.J. Berzelius Neues Allg. J. Chem. **1** (1803) 115.

[11] H. Kolbe Ann, Chem. Pharm. **49** (1847) 393.

[12] H. Vogt *Electrosynthesis of Chlorate in the Nineteenth Century* J. Electrochem. Soc. **128** (1981) 29C.

[13] P.J. Goodhew, F.J. Humphreys *Electron Microscopy and Analysis*, 2nd Edition (1988) Taylor & Francis, London, Great Britain.

[14] L. Reimer *Scanning Electron Microscopy*, 2nd Edition (1998) Springer-Verlag, Berlin, Germany.

[15] L. Reimer, H. Kohl *Transmission Electron Microscopy*, 5th Edition (2008) Springer, New York, USA.

[16] D.B. Williams, C.B. Carter *Transmission Electron Microscopy*, (1996) Plenum Press, New York, USA

[17] E. Meyer, H.J. Hug, R. Bennewitz *Scanning Probe Microscopy* (2004) Springer-Verlag, Berlin, Germany

[18] E.W. Washburn *The Dynamics of Capillary Flow* Phys. Rev. **17** (3) (1921) 273.

[19] E.P. Barrett, L.G. Joyner, P. P. Halenda *The Determination of Pore Volume and Area Distributions in Porous Substances. 1: Computations from Nitrogen Isotherms* J. Am. Chem. Soc **73** (1) (1951) 373.

[20] S. Brunauer, P.H. Emmett, E. Teller *Adsorption of Gases in Multimolecular Layers* J. Am. Chem. Soc. **60** (1938) 309.

[21] H.P. Klug and L.E. Alexander *X-ray diffraction procedures*, 2nd Edition (1974) Wiley, New York, USA.

[22] J.O. Bockris, A.K.N. Reddy, M. Gamboa-Aldeco *Modern Elecktrochemosty 2A*, 2nd Edition (2000) Kluwer Academic /Plenum Publishers, New York, USA.

[23] R.M.A. Azzam, N.M.Bashara *Ellipsometry and Polarized light*, 1st Edition (1977) North-Holland, Amsterdam, The Netherlands.

[24] J.-T. Zettler *Characterization of Epitaxial Semiconductor Growth by Reflectance Anisotropy Spectroscopy and Ellipsometry* Prog. Crystal Growth and Charact. **35** (1997) 27.

[25] S. Pizzini, G. Buzzanca, C. Mari, L. Rossi, S. Torchio *Preparation, Structure and Electrical Properties of Thick Ruthenium Dioxide Films* Mat. Res. Bul. **7** (5) (1972) 449.

[26] S. Trasatti, O.A. Petrii *Real Surface Area Measurements in Electrochemistry* Pure Appl. Chem. **63** (1991) 711.

[27] E. Guerrini, S. Trasatti *Recent Developments in Understanding Factors of Electrocatalysis* Russian J. Electrochem. **42** (2006) 1131.

[28] O.R Camara, S. Trasatti *Surface electrochemical properties of* $Ti/(RuO_2 + ZrO_2)$ *electrodes* Electrochim. Acta **41** (1996) 419.

[29] L.D. Burke, O.J. Murfhy *Cyclic Voltammetry as a Technique for Determining the Surface Area of* RuO_2 *electrodes* J. Electroanal. Chem. **96** (1979) 19.

[30] Y-.L. Chueh, C.-H Hsieh, M.-T. Chang, L.-J. Chou, C.S. Lao, J.H. Song, J.-Y Gan, Z.L. Wang RuO_2 *Nanowires and* RuO_2/TiO_2 *Core/Shell Nanowires: From Synthesis to Mechanical, Optical, Electrical, and Photoconductive Properties* Adv. Mater. **19** (2007) 143.

[31] K. Autumn, Y.A. Liang, S.T. Hsieh, W. Zesch, W.P. Chan, T.W. Kenny, R. Fearing, R.J. Full *Adhesive force of a single gecko foot-hair* Nature **405** (2000) 681.

[32] C.P. Poole, F.J. Owens *Introduction to Nanotechnology* (2003) Wiley, Hoboken, New Jersey.

[33] Y.-L. Liu, Z.-Y. Wu, K.-J. Lin, J.-J. Huang, F.-R. Chen, J.-J. Kai *Growth of single-crystalline* RuO_2 *nanowires with one- and twonanocontact electrical characterizations* Appl. Phys. Lett. **90** (2007) 013105.

[34] U. Backman, M. Lipponen, A. Auvinen, U. Tapper, R. Zilliacus, J.K. Jokiniemi *On the transport and speciation of ruthenium in high temperature oxidising conditions* Radiochim. Acta **93** (2005) 297.

[35] S.Y. Chou, P.R. Krauss, P.J. Renstrom *Imprint Lithography with 25-Nanometer Resolution* Science **272** (1996) 5258.

[36] C.M. Sotomayor-Torres, S. Zankovych, J. Seekamp, A.P. Kam, C. Clavijo-Cedeño, T. Hoffmann, J. Ahopelto, F. Reuther, K. Pfeiffer, G. Bleidiessel, G. Gruetzner, M.V. Maximov, B. Heidari *Nanoimprint lithography: an alternative nanofabrication approach* Mat. Science Eng. **C23** (2003) 23.

[37] P. Atkins, J. de Paula *Atkins' Physical Chemistry*, 7th Edition (2002) Oxford university Press, New York, USA.

[38] M. Kakihana *'Sol-Gel' Preparation of High Temperature Superconducting Oxides* J. Sol-Gel Sci. Tech. **6** (1996) 7.

[39] V. Subramanian, S.C. Hall, P.H. Smith, B Rambabu *Mesoporous anhydrous RuO2 as a supercapacitor electrode material* Solid States Ionics **175** (2004) 511.

[40] F. Rouquerol, J. Rouquerol, K. Sing *Adsorption by Powders and Porous Solids* (1999) Academic Press, London, Great Britain.

[41] R.G. Freitas, L.F. Marchesi, R.T.S. Oliviera, F.I. Mattos-Costa, E.C. Pereira, L.O.S. Bulhões, M.C. Santos *Methanol oxidation reaction on* $Ti/RuO_{2(x)}Pt_{(1?x)}$ *electrodes prepared by the polymeric precursor method* J. Power Sources **171** (2007) 373.

[42] S. Trasatti *Progress in Understanding of the mechanism of Chlorine Evolution at Oxide Electrodes* Electrochim. Acta **32** (3) (1987) 369.

[43] C.E. Vallet *Comparison of scanning probemicroscopies with RBS and SEM / EDX for the analysis of* RuO_2, TiO_2 *composites* Appl. Phys. A **65** (1997) 387.

[44] D.J. Shaw *Introduction to Colloid and Surface Chemistry*, 4th Edition (1992) Butterworth-Heinemann Ltd, Oxford, Great Britain

[45] Y.E. Roginskaya, O.V. Morozova *The role of hydrated oxides in formation and structure of DSA-type oxide electrocatalysis* Electrochim. Acta **40** (1995) 817.

[46] S. Ardizzone, M. Falciola, S. Trasatti *Effect of the nature of precursor on the electrocatalytic properties of thermally prepared ruthenium oxide* J. Electrochem. Soc. **136** (1989) 1545.

[47] E. Fachinotti, E. Guerrini, A.C. Tavares, S. Trasatti *Electrocatalysis of* H_2 *evolution by thermally prepared ruthenium oxide, effect of precursors: nitrate vs. chloride* J. Electroanal. Chem. **600** (2007) 103.

[48] J. Jirkovsky H. Hoffmannov, M. Klementov, P. Krtil *Particle size dependence of the electrocatalytic activity of nanocrystalline* RuO_2 *electrodes* J. Electrochem. Soc. **153** (6) (2006) E111.

[49] www.wikipedia.org